A balance of outward and linear inward ionic currents is required for the generation of slow wave oscillations

Jorge Golowasch[1,2], Amitabha Bose[2], Yinzheng Guan[1], Dalia Salloum[1], Andrea Roeser[1,2] and Farzan Nadim[1,2]

[1] Federated Department of Biological Sciences, New Jersey Institute of Technology and Rutgers University, Newark, NJ 07102

[2] Department of Mathematical Sciences, New Jersey Institute of Technology, Newark, NJ 07102

Abbreviated title: Slow wave oscillation require balanced currents

Corresponding Author: Jorge Golowasch

Federated Department of Biological Sciences, NJIT, 100 Summit St, CKB 337, University Heights, NJ 07103, Phone: 973-596-8444, Fax: 973-596-5689.
Email: Jorge.P.Golowasch@njit.edu

Keywords: rhythmic activity, compensation, ionic currents, model, phase space

Support: This work was supported by NSF DMS1122291 (AB), NIH MH064711 & NS085330 (JG) and NIH MH060605 (FN).

Abstract

Regenerative inward currents help produce slow oscillations through a negative-slope conductance region of their current-voltage relationship that is well approximated by a linear negative conductance. We used dynamic clamp injections of a linear current with this conductance, I_{NL}, to explore why some neurons can generate intrinsic slow oscillations whereas others cannot. We addressed this question, in synaptically isolated neurons of the crab *Cancer borealis*, after blocking action potentials. The pyloric network consists of distinct pacemaker group and follower neurons, all of which express the same complement of ionic currents. When the pyloric dilator (PD) neuron, a member of the pacemaker group, was injected with I_{NL} using dynamic clamp, it consistently produced slow oscillations. In contrast, the lateral pyloric (LP) or ventral pyloric (VD) follower neurons, failed to oscillate with I_{NL}. To understand these distinct behaviors, we compared outward current levels of PD, LP and VD neurons. We found that LP and VD neurons had significantly larger high-threshold potassium currents (I_{HTK}) than PD, and LP had lower transient potassium current, I_A. Reducing I_{HTK} pharmacologically enabled both LP and VD neurons to produce oscillations with I_{NL}, whereas modifying I_A levels did not affect I_{NL}-induced oscillations. Using phase-plane and bifurcation analysis of a simplified model cell, we demonstrate that large levels of I_{HTK} can block I_{NL}-induced oscillatory activity, whereas generation of oscillations is almost independent of I_A levels. These results demonstrate the importance of a balance between inward pacemaking currents and high-threshold K^+ current levels in determining slow oscillatory activity.

Introduction

Leak currents are key determinants of neuronal excitability (Brickley et al. 2007; Lu and Feng 2012; Lutas et al. 2016; Rekling et al. 2000) and can be regulated by many different neuromodulators, which can modify the activity to either silence neurons, or to induce spiking or oscillatory activity (Bayliss et al. 1992; Cymbalyuk et al. 2002; Egorov et al. 2002; Lu and Feng 2012; Lutas et al. 2016; Talley et al. 2000; van den Top et al. 2004; Vandermaelen and Aghajanian 1983; Xu et al. 2009). Leak currents have been proposed to control pacemaker rhythm generation (Amarillo et al. 2014; Blethyn et al. 2006; Cymbalyuk et al. 2002; Koizumi and Smith 2008; Lu and Feng 2012; Pang et al. 2009; Yamada-Hanff and Bean 2013; Zhao et al. 2010). Often, leak currents act to bring the membrane potential to within a range of voltage where other currents can activate and produce a new state of activity (Brickley et al. 2007; Lu and Feng 2012; Rekling et al. 2000; Yamada-Hanff and Bean 2013).

Regenerative inward currents, such as persistent Na^+- and low-threshold Ca^{++}-currents, are essential for the generation of oscillatory neuronal activity (Amarillo et al. 2014; Del Negro et al. 2002; Dunmyre et al. 2011; Jahnsen and Llinas 1984; McCormick and Huguenard 1992; Yamada-Hanff and Bean 2013; Zhao et al. 2010). These currents can be divided into two almost linear components, only one of which is sufficient and necessary to generate the oscillations (Bose et al. 2014; Zhao et al. 2010). Since this component is linear, we refer to it as a leak current; however, it has negative slope conductance (hence, a negative-conductance leak current, I_{NL}). It is a leak current in the sense that, when combined with the standard leak current (I_L), the total current $I_{NL}+I_L$ remains linear, and yet it is a key determinant of neuronal excitability. The mechanism by which I_{NL} controls oscillatory activity is by destabilizing the resting state of the cell (Bose et al. 2014) thereby increasing the voltage of the cell to a point where outward currents can turn on and bring the voltage back to hyperpolarized levels. In this way, when I_{NL} dominates over I_L, the total linear current can be a *de facto* pacemaker current (Bose et al. 2014; Zhao et al. 2010).

Outward currents, primarily carried by K^+, play an essential role as currents that restore the polarization of the cells from which a new cycle of depolarization and

hyperpolarization can emerge. Consequently, the kinetics of these currents are essential in determining the overall dynamics of the oscillatory activity (Bose et al. 2014). A balance between outward and inward currents is essential for the generation of oscillatory activity: too little K^+ current and the cell will be pushed towards, and sometimes locked in, a depolarized state; too much K^+ current and the increased leakiness will prevent it from escaping the hyperpolarized resting state. A growing number of recent studies indicate that ionic current levels may be linked via mechanisms involving ion channel co-regulation (Bergquist et al. 2010; Linsdell and Moody 1994; MacLean et al. 2003). A consequence of this co-regulation is that, in a population of neurons, various parameters of these different currents (most notably their amplitude or conductance) are correlated with one another (Amendola et al. 2012; Anderson et al. 2016; Anirudhan and Narayanan 2015; Goaillard et al. 2009; Golowasch 2015; Khorkova and Golowasch 2007; Roffman et al. 2012; Schulz et al. 2006; Schulz et al. 2007; Srikanth and Narayanan 2015; Temporal et al. 2012; Temporal et al. 2014). Such co-regulation is likely to be involved in maintaining the balance of regenerative and outward ionic currents to regulate activity levels in oscillatory neurons.

In the stomatogastric nervous system, I_{NL}, corresponding to the negatively sloped portion of the modulator-activated inward current I_{MI} (Golowasch and Marder 1992b; Gray and Golowasch 2016; Swensen and Marder 2000), is a pacemaker current of the pyloric network pacemaker neurons (Bose et al. 2014; Zhao et al. 2010). This current underlies the slow oscillations observed in the presence of a variety of neuromodulators (Golowasch and Marder 1992b; Swensen and Marder 2000), even in the presence of the Na^+ channel blocker tetrodotoxin. Although I_{MI} is expressed by all pyloric neurons (Swensen and Marder 2000), when these neurons are synaptically isolated, modulator-induced oscillations occur only in a small subset: the three electrically coupled neurons regarded as the pacemaker neurons of the network (two Pyloric Dilators, PD, and one Anterior Burster, AB, neurons (Hooper and Marder 1987)). Why other pyloric neurons do not show pacemaker activity in the presence of modulators is unclear.

Using both theoretical and experimental methods, we test the hypothesis that the generation of slow-wave oscillations requires the correct balance of a linear pacemaker

inward current and outward currents. Our hypothesis is based on the property that I_{NL} is sufficient to emulate the pacemaker I_{MI} (Bose et al. 2014). We show that this balance can only be produce in a subset pyloric network neurons that express the appropriate levels of high-threshold potassium currents. We further show how the induction of oscillatory activity depends on the interplay between the maximal conductance (g_{NL}) and equilibrium potential (E_{NL}) of I_{NL}, and how these observations match our theoretical predictions.

Methods

Experimental

Experiments were performed on identified neurons from the stomatogastric ganglion (STG) of male crabs (*Cancer borealis*). The animals were obtained at local markets in Newark (NJ) and maintained in seawater tanks at 10–13°C. The entire stomatogastric nervous system, including the anterior commissural and esophageal ganglia, STG and connecting and motor nerves were dissected out as previously described (Selverston et al. 1976) and pinned down on a Sylgard-coated Petri dish, and the STG was desheathed, to allow for electrode impalement of the cell bodies. All preparations were continuously superfused with chilled (10 - 13°C) physiological *Cancer* saline: (in mM) 11 KCl, 440 NaCl, 13 $CaCl_2$, 26 $MgCl_2$, 11.2 Trizma base, 5.1 maleic acid, pH 7.4 –7.5.

Extracellular recordings were performed with pin electrodes placed in petroleum jelly wells built around individual nerves and recorded differentially, relative to an electrode placed outside of the well, using an A-M Systems 1700 differential amplifier (A-M Systems, Carlsberg, WA). Intracellular recordings, current injections and voltage clamp were performed with Axoclamp 2B amplifiers (Molecular Devices, Sunnydale, CA) using double impalements with 0.6 M K_2SO_4 + 20 mM KCl-filled borosilicate electrodes. Low resistance electrodes (15-20 MΩ) were used for current injection, and high resistance electrodes (30-40 MΩ) for voltage measurement. Individual neurons were identified by matching intracellularly recorded action potentials to action potentials on identified motor nerves that innervate known muscles (Selverston et al. 1976).

In every preparation, action potentials were blocked by bath application of 10^{-7} M tetrodotoxin (TTX; Biotium). This treatment effectively blocks all modulatory inputs, including peptidergic and cholinergic modulators that activate I_{MI} (Golowasch and Marder 1992b; Swensen and Marder 2000), therefore decentralizing the preparation.

The dynamic clamp technique was used to activate I_{NL} (Fig. 1A, red) or a cut-off version of I_{NL} that does not cross the current axis (Fig. 1A, blue) and thus corresponds to a more realistic version of the negative-slope component of I_{MI} (Fig. 1A, gray trace). A variety of values of I_{NL} parameters (Zhao et al. 2010) was tested. The dynamic clamp was implemented using the NetClamp software (Gotham Scientific http://gothamsci.com/NetClamp) on a 64 bit Windows 7 PC using a NI PCI-6070-E board (National Instruments).

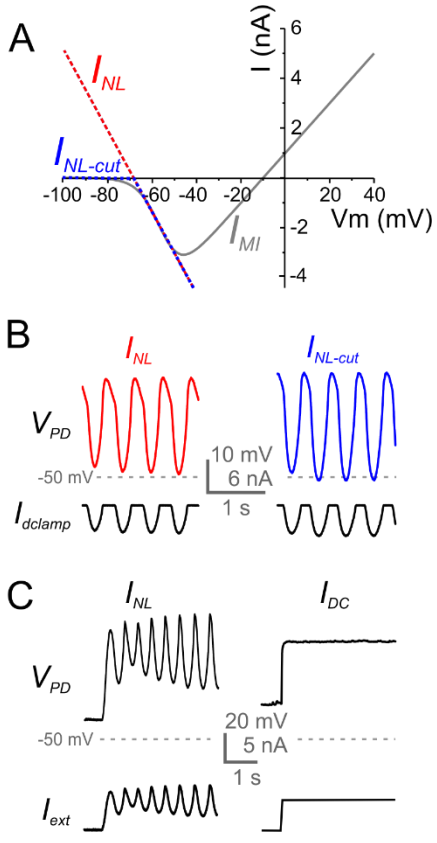

Figure 1. *Effect of I_{NL} injection in PD neurons*. **A**. The I-V curves of I_{MI} (gray), I_{NL} (red) and the truncated version of I_{NL} ($I_{NL\text{-}cut}$, blue). Note that both I_{NL} and $I_{NL\text{-}cut}$ are good approximations to the negatively sloped portion of I_{MI}, where

$$I_{MI} = g_{MI} m_{\infty}(v)[v - E_{MI}], \quad m_{\infty}(v) = \frac{1}{1 + e^{-[v+10]/6}}$$

B. Effect of dynamic clamp injection of I_{NL} (left) and $I_{NL\text{-}cut}$ (right) on the activity of PD neurons. Both traces are from the same neuron. Bottom traces show the current injected by the dynamic clamp (I_{dclamp}). **C**. Injection of I_{NL} (left) and comparison with injection of constant current of the same time-averaged amplitude (right) as I_{NL}. Different preparation as in B.

Data acquisition was performed using a Digidata 1332A data acquisition board and the pClamp 10.3 software (Molecular Devices). Injections of current in dynamic clamp were

performed at 10 KHz and voltage recordings at 5 KHz. The following equations were used:

$$I_{NL} = g_{NL}[v - E_{NL}]$$
$$I_{NL-cut} = g_{NL}[v - E_{NL}]Heav(v - E_{NL})$$

For dynamic clamp experiments involving the pyloric dilator (PD) neuron, the values used for injection were 12 values of g_{NL} from -0.01 to -0.30 µS and the reference value of E_{NL} was set at 2 mV below the cell's resting potential (V_{rest}), typically resulting in E_{NL} = −67 to −58 mV. The value of E_{NL} was changed by increments of ±5 mV up to ±15 mV from this reference value (a total of 7 values).

Ionic currents were measured in two-electrode voltage clamp. The high-threshold K^+ current (I_{HTK}) was measured with depolarizing voltage steps from a holding voltage of -40 mV to inactivate the transient K^+ current (I_A). I_A was measured with the same depolarizing voltage steps as for I_{HTK} but from a holding voltage of -80 mV and calculated by subtraction of I_{HTK} from these recordings (Zhao and Golowasch 2012).

Pharmacological agents were prepared immediately before use. Statistical analysis was performed with either SigmaPlot 12 (Systat) or Origin 8.5 (OribinLab) software.

Model

The equations that describe the full model involve currents for leak (I_L), negative-conductance leak with cutoff ($I_{NL\text{-}cut}$) and three potassium currents, delayed rectifier (I_{Kdr}), high-threshold (I_{HTK}) and an A-current (I_A) are:

$$\begin{aligned} C\frac{dv}{dt} &= I_{ext} - g_L[v - E_L] - g_{NL}[v - E_{NL}]Heav\left(v - E_{NL}\right) - g_{Kdr}w[v - E_K] \\ &\quad - g_{HTK}m_\infty(v)[v - E_K] - g_A wh[v - E_K] \\ \frac{dw}{dt} &= \frac{w_\infty(v) - w}{\tau_K(v)}, \\ \frac{dh}{dt} &= \frac{h_\infty(v) - h}{\tau_A(v)} \end{aligned} \qquad (1)$$

The parameter C is the capacitance. The variable v represents the membrane potential, w is an activation variable for potassium currents which, for convenience, is taken to be common for both I_{Kdr} and I_A, and h is an inactivation variable for I_A. I_{HTK} is considered to have instantaneous activation and no inactivation. The parameters g_x and E_x represent the maximal conductance and reversal potentials for the various currents, respectively. We use the cutoff version $I_{NL-cut} = g_{NL}[v - E_{NL}]Heav(v - E_{NL})$ with a negative maximal conductance value g_{NL} (Fig. 1A, blue). The Heaviside function $Heav(v - E_{NL})$, is 0 when $v < E_{NL}$ and is equal to 1 when $v \geq E_{NL}$. This implies that for $v \geq E_{NL}$, $I_{NL\text{-}cut}$ is simply a linear current with negative conductance, while for $v < E_{NL}$, $I_{NL\text{-}cut} = 0$ (Fig. 1A, blue). The terms $w_\infty(v)$ and $m_\infty(v)$ are the steady-state activation functions for the two potassium currents and $h_\infty(v)$ is the steady state inactivation function of I_A. They are described by equations:

$$w_\infty(v) = \frac{1}{1+\mathrm{e}^{-(v+40)/4}}, \quad m_\infty(v) = \frac{1}{1+e^{-(v+25)/3}}, \quad h_\infty(v) = \frac{1}{1+\mathrm{e}^{-(v+50)/4}} \quad .$$

The associated time constants are given by

$$\tau_K(v) = \frac{3.9}{\cosh((v+40)/4))}, \quad \tau_A(v) = \frac{16.25}{\cosh((v+50)/4))} .$$

Parameter values that vary across simulations are provided in the Results, while those that were fixed are given here: C = 1 μF/cm^2, g_L = 0.00325 μS, E_L = -60 mV, g_{Kdr} = 0.0325 μS, E_K = -80 mV and I_{ext} = 0.065 nA. These parameters were chosen so that the period of oscillations in the simulations was on the order of those found in experiments. Simulations and bifurcation diagrams were constructed using XPPAUT (Ermentrout 2002).

In prior work (Bose et al. 2014), we analyzed the case of $I_{HTK} = I_A = 0$ and showed that non-zero I_{NL} and I_{Kdr} currents alone can produce oscillations. In order to now isolate the effect of I_{HTK} with regard to pacemaker properties, for much of the analysis we continue to keep I_A=0. With I_A=0, the variable h is redundant and the set of equations (1) reduces to a two-dimensional system that will be analyzed using phase plane methods. We will

show that a non-zero value of I_A does not affect the existence of oscillations, but that if it is large enough it can introduce a stable, sub-threshold fixed point.

Results

The pacemaker current operates over restricted parameter ranges

Our first goal here is to characterize some of the conditions that I_{MI} needs to satisfy to operate as a pacemaker current as predicted by our previous theoretical work (Bose et al. 2014). Oscillatory activity can be induced in the PD neuron by injecting the negative-leak conductance current I_{NL} (Fig. 1B, C), which is a linearized version of the pacemaker current I_{MI} (Fig. 1A). The effect of I_{NL} only depends on the region of its I-V curve where the current is negative. Therefore, injection of the same current which is set to 0 below E_{NL} (the cut-off version $I_{NL\text{-}cut}$) produces almost identical oscillations (Fig. 1B; see Methods). Since the results for oscillatory activity are nearly identical, henceforth we use I_{NL}.

The effect of I_{NL} in producing oscillations in the PD neuron could not be mimicked by injecting a depolarizing DC current (Fig. 1C right) equal to the time-averaged current measured during the dynamic clamp injection of I_{NL} (Fig. 1C left), demonstrating that the effects of I_{NL} are not simply a consequence of a depolarization of the cell by I_{NL}, but its role as a voltage-dependent current.

In our previous study, we predicted that oscillations produced by I_{NL} would occur in a restricted range of g_{NL} (Bose et al. 2014). To explore the effect of the I_{NL} parameters on the oscillatory activity, we changed g_{NL} over 12 values from -0.01 to -0.30 µS and E_{NL} over a range of ±15 mV in steps of ±5 mV from the initial reference value (for a range of 12 x 7 = 84 runs; see Methods). We found that there was a double Gaussian distribution (R^2=0.9185) of g_{NL}-E_{NL} values over which I_{NL} was effective in eliciting oscillatory activity (Fig. 2A).

An important point that these results illustrated was that oscillatory activity in the pyloric pacemaker cells does not require TTX-sensitive Na^+ currents to be produced. We

observed a relative independence of cycle period on g_{NL} (Fig. 2B), but a decreasing amplitude of oscillations as g_{NL} became larger in absolute value (Fig. 2C). On the other hand, period was an increasing function of E_{NL} (Fig. 2D) and the oscillation amplitude had an inverted U-shape relationship with E_{NL} (Fig. 2E).

Pacemaker cells balance inward and outward currents to produce oscillatory activity

The effect of I_{HTK}

As we have seen, I_{NL} injected into neurons of the pacemaker group (i.e. PD neurons) consistently induces oscillatory activity (Fig. 2, Fig. 3, top left), albeit within relatively narrow ranges of g_{NL} and E_{NL} (Fig. 2). We examined whether follower neurons in the network were equally capable of generating oscillatory activity.

We observed that none of the follower cells in the pyloric network (ventral dilator VD, pyloric constrictor PY, inferior cardiac IC, lateral pyloric LP and lateral posterior gastric LPG neurons) were capable of generating consistent oscillatory activity independently of the combination of g_{NL} and E_{NL} used. Individual examples shown in Figure 3 were obtained by injection of g_{NL} = -0.16 μS and $E_{NL} = V_{rest} – 2$ mV for each cell type. However, each cell was further tested with the same combination of g_{NL} and ΔE_{rev} as the PD cells shown in Figure 2A. We found that only one out of eight LP neurons tested expressed any oscillatory activity, and none of the other follower cells tested could express such activity for any of the g_{NL} and E_{NL} combinations.

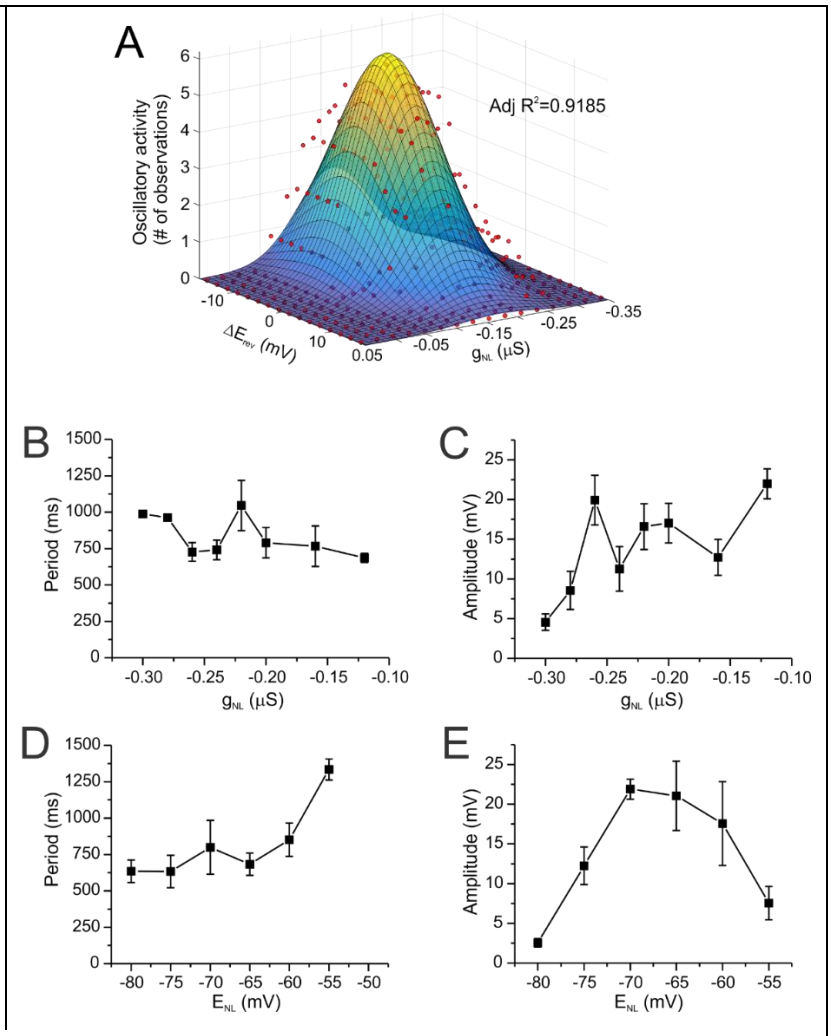

Figure 2. *Effect of I_{NL} parameters on PD neuron oscillations*. Identified PD neurons (N=7) were injected with dynamic clamp I_{NL} and parameters g_{NL} and E_{rev} were modified over a broad range of values. **A**. The presence or absence of oscillations (# of oscillatory preparations out of 7) was graphed as a function of the change in E_{rev} relative to each cell's resting voltage (ΔE_{rev} = 0 = V_{rest} – 2 mV), and the value of the negative conductance injected (g_{NL}). Red symbols are the experimental data. The smooth surface is a Gaussian surface fit to the experimental data. Adjusted R^2 = 0.9185. **B**. Average period vs g_{NL}. **C**. Average amplitude vs g_{NL}. **D**. Average period vs E_{NL}. **E**. Average amplitude vs E_{NL}. All data shown in A-E are from the same set of cells. Error bars are SEM.

To understand what prevents follower cells from expressing oscillatory activity, we examined the levels of K^+ currents expressed in two of the follower cells (LP and VD neurons) and compared that to the current levels expressed by the pacemaker PD neurons. Our hypothesis throughout was that large outward currents could be responsible for preventing oscillatory activity. Figure 4 shows the comparison of two outward currents, I_{HTK} and I_A (see definitions in Methods), with I_{HTK} further divided into peak (I_{HTK} peak) and steady state (I_{HTK} SS) in two cell types the PD and LP neurons.

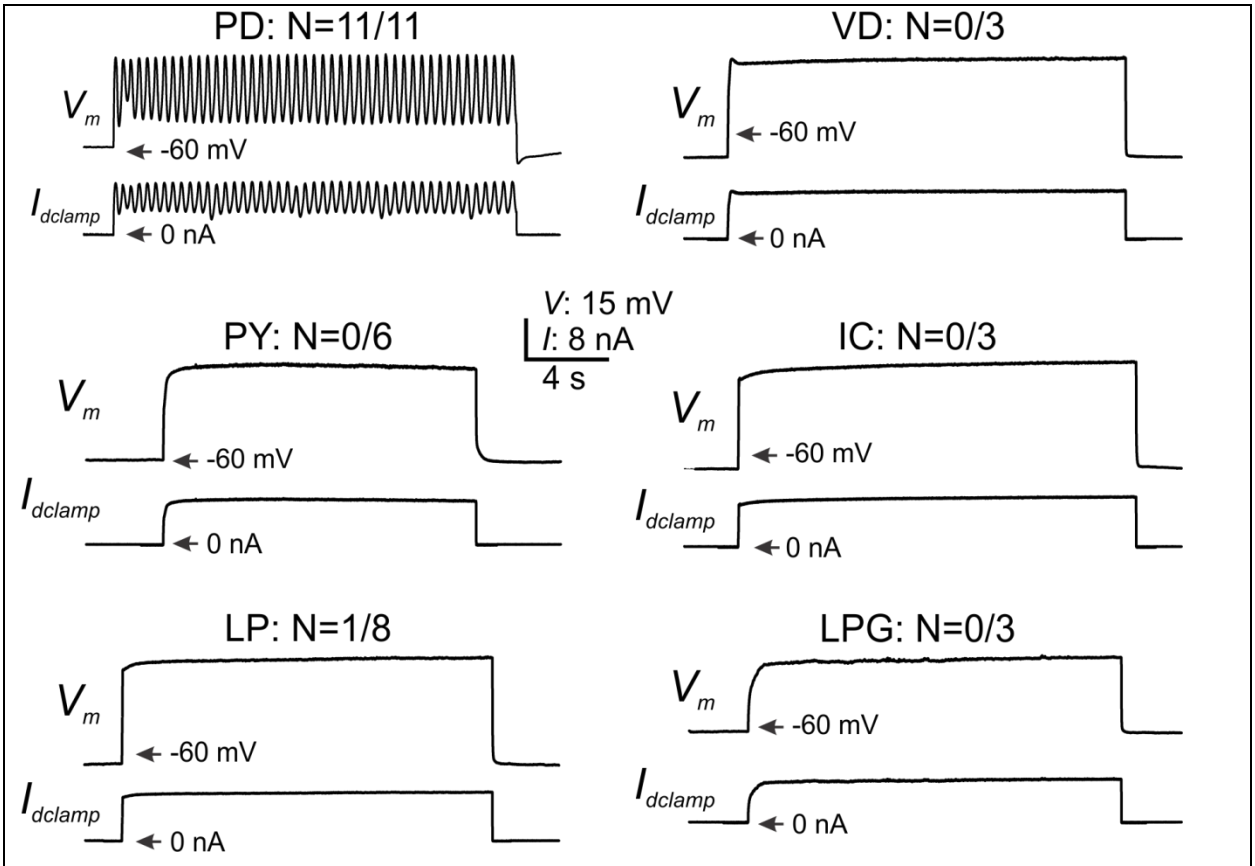

Figure 3. D*ynamic clamp I_{NL} injection in pyloric network neurons cannot induce oscillatory activity in follower cells*. Identified neurons with characteristic activity response to I_{NL} injection (g_{NL} = 0.16 μS, E_{NL} = V_{rest} – 2 mV) of the cells listed. PD neurons responded with oscillatory activity in 100% of the preparations tested. The numbers next to the cell type name indicate how many of the total cells tested showed any oscillatory activity. All cells were tested with the same combinations of g_{NL} and ΔE_{rev} as the PD neurons shown in Figure 2A. Top traces in each panel is the membrane potential; bottom trace is the dynamic clamp current injected.

PD neurons expressed a significantly smaller I_{HTK} than LP neurons, when this current was compared at its peak (two-way ANOVA, P = 0.029, Fig. 4B), as well as at steady state (P < 0.001, Fig. 4C). Interestingly, the activation parameters as well as the maximal conductance of the peak of I_{HTK} are not significantly different between PD and LP neurons (Fig. 4E; PD, Table 1). However, the differences, especially in g_{max_HTK} and $V_{1/2\_HTK}$, while independently not significantly different between these cells, were sufficient to make the currents different between them.

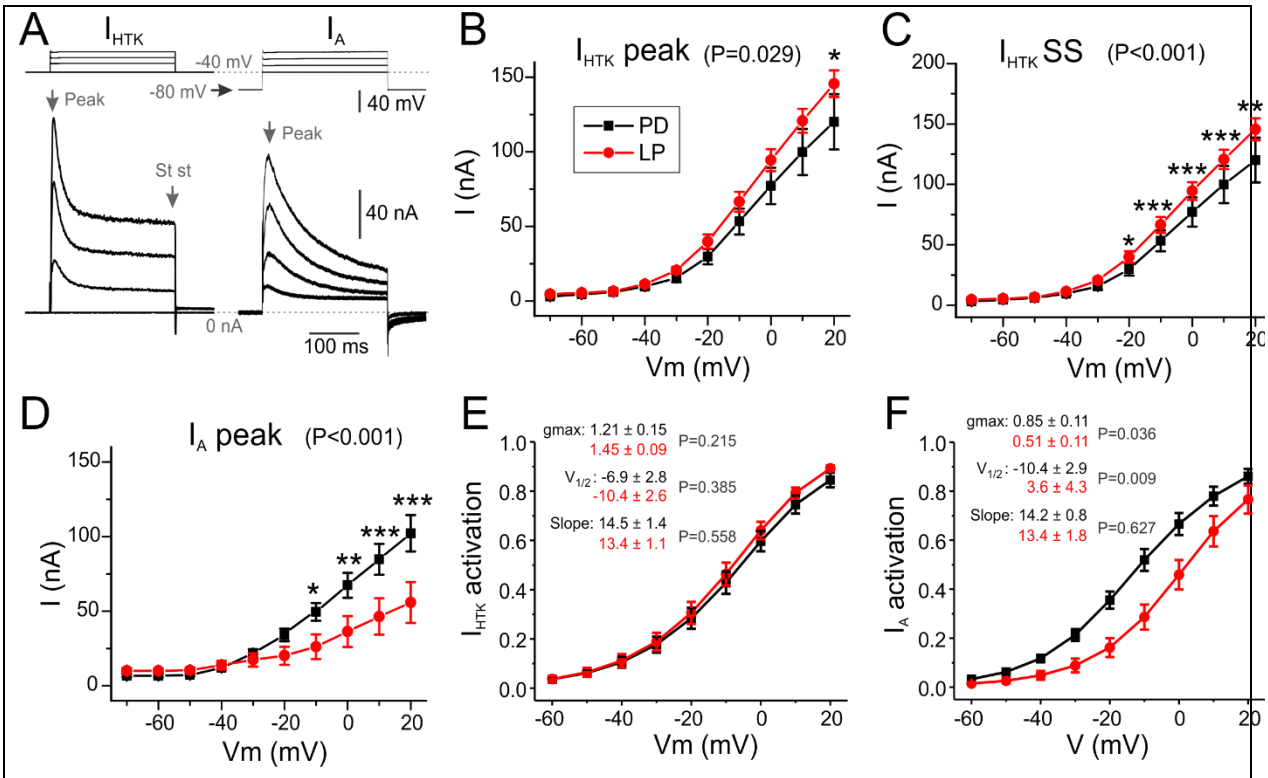

Figure 4. *Potassium current levels in two key pyloric network neurons*. **A**. Sample traces of I_{HTK} (left) and I_A (right). Grey vertical arrows point to the times at which I_{HTK} *peak*, I_{HTK} *SS* and I_A are measured. **B**. I-V curves of the peak of the high threshold current I_{HTK}. The curves are significantly different (Two-way ANOVA, P < 0.029). **C**. Steady state I-V curves of I_{HTK}. The curves are significantly different (Two-way ANOVA, P < 0.001). Asterisks indicate the source of the difference from two-way ANOVA analysis and Tukey pairwise comparisons (* P < 0.05; ** P < 0.01; *** P < 0.001). **D**. I-V curves of the peak of the transient K^+ current I_A. The curves are significantly different (Two-way ANOVA, P < 0.001).). Data for PD neurons in black and red for LP neurons. **E**. Activation curves for I_{HTK} peak and the shown parameters are calculated as in D. **F**. Average of the voltage-dependent activation curves of I_A derived from the I-V curves of each cell used in A. The I-V curves were fitted with the equation.

$I = g_{\max} \frac{1}{1+e^{[v_{1/2}-v]/slope}}[v-E]$. *E* was fixed at -80 mV and the other three parameters were determined from the fit ($V_{1/2}$ and *slope* in mV, g_{max} in μS. P values are for Students t-test analysis for each parameter between the two cells. All error bars are SEM.

Table 1. I_{HTK} and I_A parameters in PD and LP neurons. Parameters were obtained from fits of a sigmoidal function to conductances calculated from I_{HTK} and I_A measurements and a driving force = (V_m - E_{rev}), with E_{rev} = -80 mV.

	Mean		SD		t (d.f.)	P
	PD	LP	PD	LP		
g_{max_HTK} (μS)	1.21	1.45	0.61	0.33	-1.270 (28)	0.215
$V_{1/2\_HTK}$ (mV)	-6.9	-10.4	11.6	9.3	0.883 (28)	0.385
V_{slope_HTK} (mV)	14.5	13.4	5.8	3.8	0593 (28)	0.558
g_{max_A} (μS)	0.85	0.51	0.44	0.39	2.205 (28)	0.036
$V_{1/2\_A}$ (mV)	-10.4	3.6	11.8	15.7	-2.829 (28)	0.009
V_{slope_A} (mV)	14.2	13.5	3.4	6.5	0.491 (28)	0.627

In contrast to I_{HTK}, PD neurons had a significant larger I_A than LP neurons (two-way ANOVA, P = 0.001, Fig. 4D) in part derived from a significantly more hyperpolarized activation curve ($V_{1/2\_A}$, Fig. 4F, Table 1) and a significantly higher maximum conductance (g_{max_A},Table 1). The V_{slope} of I_A did not differ significantly between the two cells (Table 1).

The functional significance of K^+ current amplitude differences

In order to test if the differences in K^+ current levels reported above are functionally related to the inability of follower cells to generate oscillatory activity when injected with I_{NL}, we reduced I_{HTK} with different concentrations of TEA (Golowasch and Marder 1992a) in the LP neuron. A significant effect of TEA on the I_{HTK} I-V curve is observed at all voltages (two-way RM ANOVA, P = 0.008, Fig. 5A). In fact, a highly significant effect of TEA concentrations was observed, with a maximum inhibition level of ~80% and a half-maximal effect at 1.6 mM (Fig. 5B). We tested whether reduced I_{HTK} conditions were more permissive for producing oscillations by injecting I_{NL} (g_{NL} = -0.16 μS) in the presence of 8 mM TEA. We observed that, under these conditions, oscillatory activity could be consistently elicited in the LP neuron (Fig. 5C; N = 4) comparable to those

generated by PD neurons (compare with Fig. 1B, C). As with PD neurons (see Fig. 1C), DC injections could not trigger oscillatory activity in LP neurons (Fig. 5D).

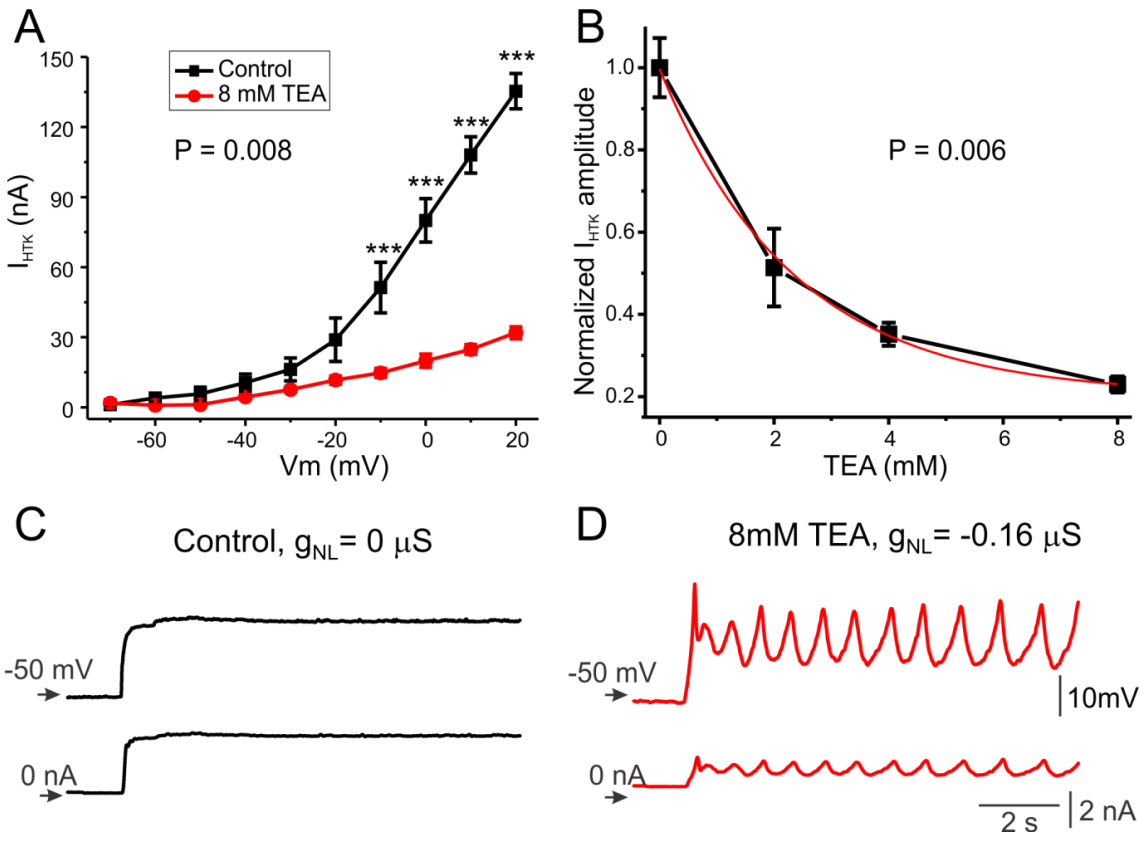

Figure 5. *High I_{HTK} levels are responsible for the inability of LP neurons to generate oscillatory activity*. **A.** I-V curves of the peak I_{HTK} in LP neurons under control (0 mM TEA, black) and 8 mM TEA (red). A significant decreases is observed overall (Two-way RM ANOVA, N = 3, P = 0.008) with asterisks indicating the source of the difference from Tukey pairwise comparisons (*** P < 0.001). **B**. Dose-dependent sensitivity of peak I_{HTK} to TEA. *I_{HTK} peak* was normalized to the current measured in control (0 mM TEA). Average ± SEM is plotted. The overall effect was statistically significant (One-way RM ANOVA, N = 3, P = 0.006). The red trace is an exponential fit with a saturation level at ~20%, and an ID_{50} = 1.6 mM. **C**. Effect of dynamic clamp injection of I_{NL} (g_{NL} = -0.16 µS; E_{NL} = -52 mV). Top trace is membrane potential, bottom trace is current injected by the dynamic clamp circuit. **D**. Effect of injection of DC equal to the time-averaged current during I_{NL} injection shown in C.

The effect of I_A current amplitude differences

Because I_A also shows significantly different levels in PD neurons compared to the LP neuron, albeit with higher levels in the PD neuron (Fig. 4A), we tested the effect of modifying I_A using the blocker 4-AP in PD neurons. We expected that, if I_A is involved in

the regulation of PD neurons to generate oscillatory activity, reducing I_A levels in the PD neuron would affect its oscillatory properties. Figure 6 shows that 1 mM 4-AP significantly affects I_A overall (two-way ANOVA, P = 0.012 for 4-AP treatment), reducing it to levels similar to those measured in LP neurons, i.e. ~50% at all voltages tested (see Fig. 4A). Yet, applying 1 mM 4-AP had virtually no effect on the ability of these cells to oscillate in response to I_{NL} injection (compare Fig. 6B control with similar injection in the presence of 1 mM 4-AP in Fig. 6C).

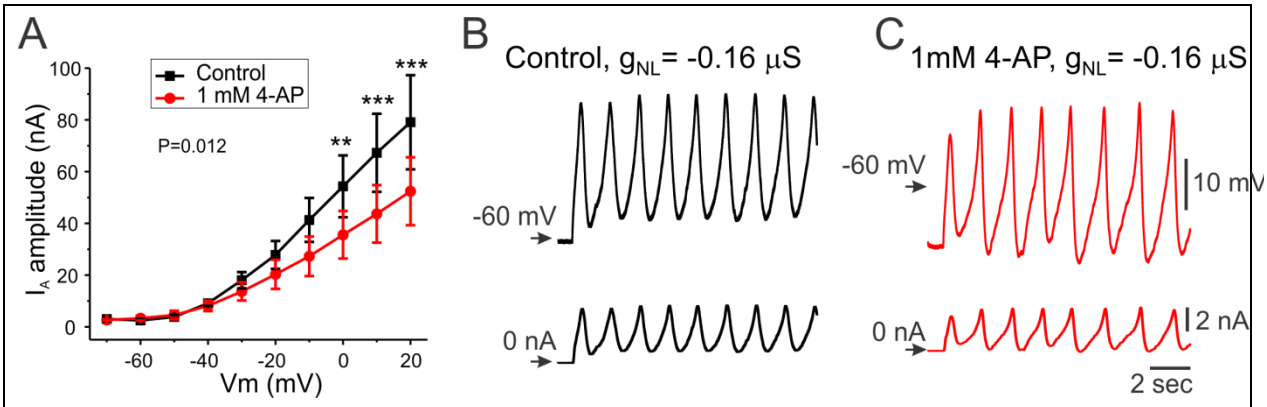

Figure 6. *I_A does not appear to be involved in the ability of PD neurons to generate oscillatory activity*. **A.** I-V curves of the peak I_A in PD neurons under control (0 mM 4-AP, black) and 1 mM 4-AP (red). A significant decrease is observed overall (Two-way RM-ANOVA, N = 3, P = 0.012) with asterisks indicating the source of the difference using Tukey pairwise comparisons (** P < 0.01, *** P < 0.001). **B**. Effect of dynamic clamp injection of I_{NL} in the absence of 4-AP (g_{NL} = -0.16 µS; E_{NL} = -72 mV). Top trace is membrane potential, bottom trace is current injected by the dynamic clamp circuit. **C**. Effect of dynamic clamp injection of I_{NL} in the presence of 1 mM 4-AP (g_{NL} = -0.16 µS; E_{NL} = -72 mV).

Similar results were observed when comparing the PD and VD neurons, the latter another follower cell in the pyloric network. I_{HTK} in PD neurons was found to be significantly lower in amplitude across its voltage activation range than in VD neurons (two-way ANOVA, P = 0.001, Fig. 7A), whereas, unlike the comparison of PD and LP neurons, there was no significant difference in I_A between these two cells (two-way ANOVA, P = 0.787, Fig. 7B).

Table 2. I_{HTK} and I_A parameters in PD and VD neurons. Parameters were obtained from fits of a sigmoidal function to conductances calculated from I_{HTK} and I_A measurements and a driving force = (V_m - E_{rev}), with E_{rev} = -80 mV.

	Mean		SD		t (d.f.)	P
	PD	VD	PD	VD		
g_{max_HTK} (μS)	1.37	2.22	0.66	1.21	-1.894 (15)	0.078
$V_{1/2\_HTK}$ (mV)	-11.9	-13.5	9.8	13.5	0.274 (15)	0.788
V_{slope_HTK} (mV)	16.8	14.9	6.1	6.0	0.605 (15)	0.554
g_{max_A} (μS)	1.06	0.81	0.41	0.47	1.183 (15)	0.255
$V_{1/2\_A}$ (mV)	-12.5	-19.2	12.3	15.8	0.974 (15)	0.345
V_{slope_A} (mV)	14.6	9.2	2.8	3.7	3.366 (15)	0.004

Bath application of 8 mM TEA reduced the amplitude of I_{HTK} significantly (Fig. 7C, N=4, two-way RM-ANOVA, P = 0.003). The effect of TEA was dose-dependent (one-way RM-ANOVA, P < 0.001, Fig. 7D). When I_{NL} was injected (g_{NL} = -0.16 μS) in control medium (0 mM TEA), VD neurons such as the one shown in Figure 7E depolarized but never generated oscillations (see also Fig. 3). However, in the presence of 8 mM TEA, the same I_{NL} injection elicited oscillations (Fig. 7F) comparable to those produced by I_{NL} in PD neurons in normal TTX saline (Fig. 1B, C) and LP neurons in TEA (Fig. 5D).

Modeling description of experimental observations

We performed simulations using equation (1) to determine whether a theoretical model provides a framework for understanding our experimental findings. The main question we investigated was whether differences in various K^+ currents could cause a model neuron to either oscillate or not. Additionally, we checked to see what computational predictions our model made with regards to period and amplitude as functions of parameters associated with I_{NL}.

To guide the simulations, we first discuss the phase space structure of the model. Recall that we are keeping g_{Kdr} fixed throughout at 0.0325 μS, and g_L at 0.00325 μS. This is to ensure oscillations in the absence of additional K^+ currents when I_{NL} is added.

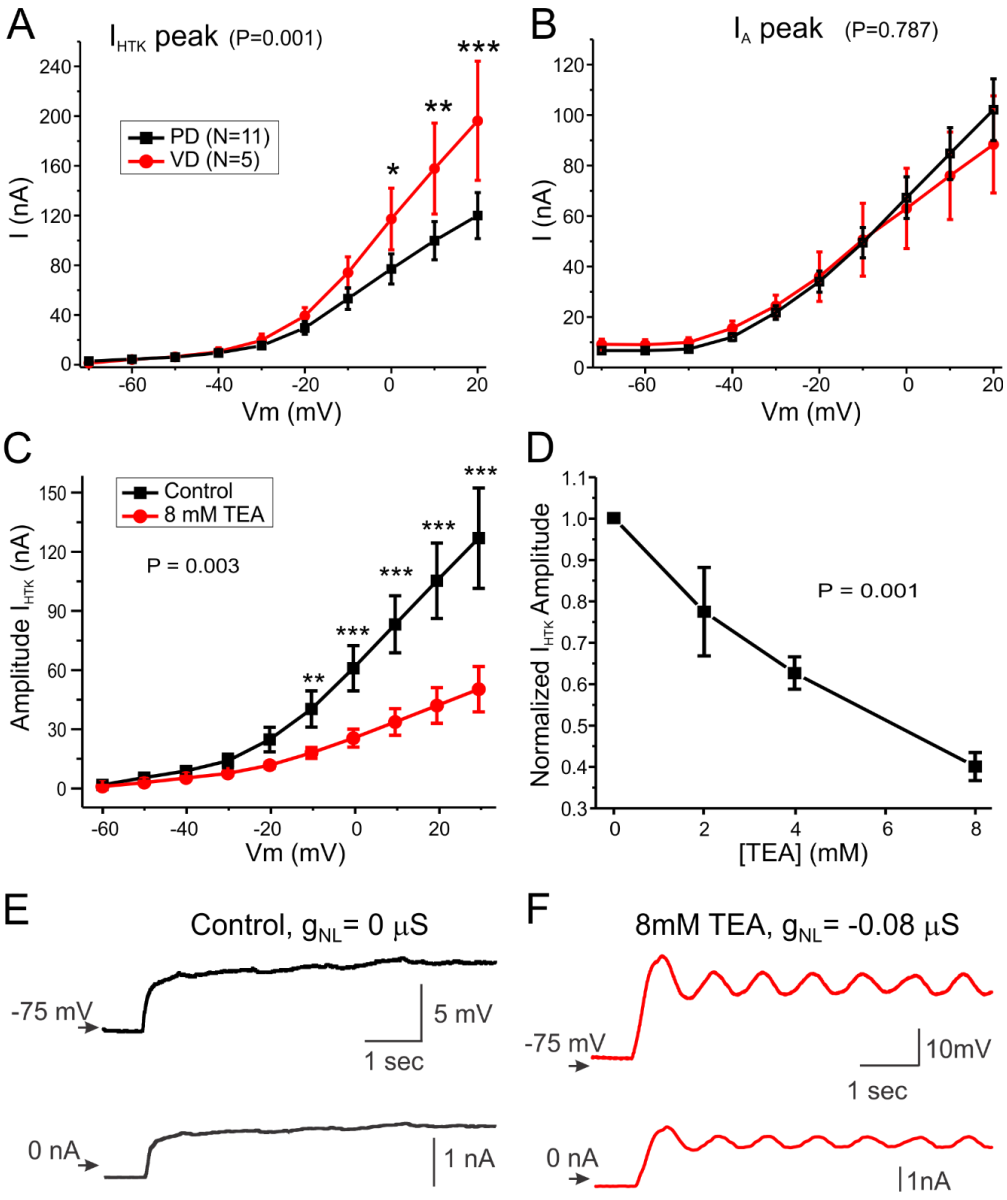

Figure 7. *High I_{HTK} levels are responsible for the inability of VD neurons to generate oscillatory activity*. **A.** I-V curves show that the peak I_{HTK} in VD neurons is almost twice as large as in PD neurons (Two-way ANOVA, P = 0.001) over most of its activation range. **B**. I-V curves of I_A show no significant difference between PD and VD neurons (Two-way ANOVA, P = 0.787). **C.** I-V curves of the peak I_{HTK} in VD neurons under control (0 mM TEA, black) and 8 mM TEA (red). A significant decrease is observed overall (Two-way RM ANOVA, N = 4, P = 0.003) with asterisks indicating the source of the difference from a Tukey pairwise comparisons. * P < 0.05** P < 0.01; *** P < 0.001). **D**. Sensitivity of $I_{HTK\text{-}peak}$ to TEA. $I_{HTK\text{-}peak}$ was normalized to the current measured in control (0 mM TEA). Average ± SEM is plotted. The overall reduction of $I_{HTK\text{-}peak}$ by TEA was significant (One-way RM ANOVA, N = 4, P = 0.001). **E, F**. Effect of dynamic clamp injection of I_{NL} (g_{NL} = -0.08 µS; E_{NL} = -70 mV) in normal saline (**E**) and in the presence of 8 mM TEA (**F**). Top trace is membrane potential, bottom trace is current injected by the dynamic clamp circuit.

Now we examine the role of other K^+ currents known to be expressed in most neurons, and in pyloric neurons in particular. When $I_A = 0$, the model equations involve only the v and w variables, allowing for phase plane analysis. The nullclines of equation (1) are obtained by plotting the set of points that satisfy $v'=0$ and $w'=0$, respectively. The v-nullcline is decreasing for $v < E_{NL}$. If $|g_{NL}|$ is sufficiently large relative to g_L, then the nullcline can increase for a range of values $v \geq E_{NL}$. The w-nullcline is a monotone increasing sigmoidal function. If it intersects the v-nullcline along its decreasing portion, then a stable fixed point ensues and oscillations are not possible. If the intersection of the two nullclines occurs for $v \geq E_{NL}$ then oscillations may be possible and depends on the slope of each at the point of intersection. We will show that, as g_{HTK} is increased, oscillatory behavior is destroyed.

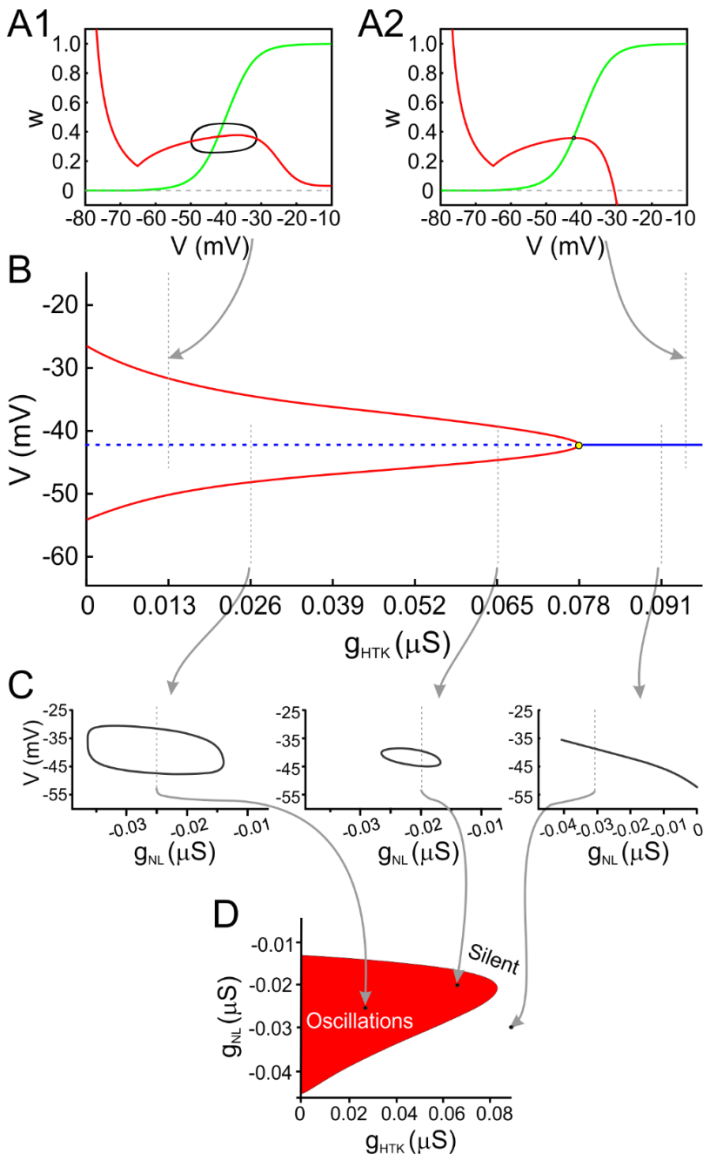

Figure 8 *The effect of I_{HTK} on the existence of oscillations*. **A**. Panel A1 shows the v-w phase plane for low values of g_{HTK} in which an oscillatory solution exists. For larger values of g_{HTK} the oscillatory solution fails to exist, as shown in panel A2, because the stronger I_{HTK} stabilizes the fixed point at the intersection of the two nullclines. **B**. Bifurcation diagram showing how the existence and amplitude of oscillatory solutions depends on g_{HTK}. Arrows from panels A1 and A2 show the values of g_{HTK} used to produce those simulations. Oscillatory solutions are lost through a Hopf Bifurcation as g_{HTK} increases. **C**. Bifurcation diagrams showing behavior of solutions at gixed values of g_{HTK} while g_{NL} is varied. The range of g_{NL} values for which oscillations exist decreases at g_{HTK} increases (compare left and middle diagrams). If g_{HTK} is too large (rightmost diagram), no amount of g_{NL} can restore oscillations. **D**. Bifurcation diagram summarizing behavior in the g_{HTK}- g_{NL} parameter space. Oscillations are possible for parameter values in the red region bounded between the parabola-like shape and the vertical axis and are not possible outside of that region.

Figure 8A1 shows phase plane from equation (1) when g_{NL} = -0.0195 µS, g_{HTK} = 0.013 µS and g_A = 0 µS. For this choice of parameters, the *w*-nullcline intersects the *v*-nullcline along a portion where the latter is increasing with a sufficiently large slope at the point of intersection. This produces an unstable fixed point. A periodic solution surrounds this unstable fixed point because, as *v* becomes too hyperpolarized, I_{NL} current drives the voltage away from E_{NL}. At larger values of *v*, I_{Kdr} activates and restricts the voltage from increasing too much. This result is consistent with our prior work (Bose et al. 2014) in which I_{HTK} was not present. Thus, the addition of this small amount of *HTK* conductance does not play a role in the generation of oscillations, but it does limit the amplitude at both higher and lower values of *v*. Indeed, the largest amplitude oscillation under these conditions exists when g_{HTK} = 0 (Fig. 8B).

We then increased the value of g_{HTK} to 0.0975 µS. Figure 8A2 shows the ensuing phase plane. Note that the only change is that the *v*-nullcline now has a much steeper and pronounced right branch along which it is decreasing. Moreover, the slope of the *v*-nullcline at the intersection with the *w*-nullcline has decreased enough to stabilize that fixed point. This change is indicative of a Hopf bifurcation, which in fact occurs as g_{HTK} is increased. Figure 8B shows that as g_{HTK} is increased from lower values, the periodic solution decreases in amplitude (upper and lower bounds of oscillations shown by solid red curves). Moreover, the unstable fixed point (dashed blue curve) gains stability through a Hopf bifurcation near g_{HTK} =0.078 µS and oscillations cease to exist. The reason for this loss of excitability is that I_{HTK} is too strong and destroys the balance between I_{Kdr} and $I_{NL\text{-}cut}$ that could produce oscillations. In short, too much I_{HTK} is incompatible with the production of oscillations. This finding is consistent with our experimental results shown in Figs. 5 and 6.

We next varied g_{NL} to further understand the relationship between these currents. Figure 8C shows bifurcation diagrams for three different fixed values of g_{HTK}, indicated by arrows from Fig. 8B, as we vary g_{NL}. The rightmost panel shows that if g_{HTK} is too large, then no amount of $I_{NL\text{-}cut}$ can produce oscillations. Indeed for all values of g_{NL}, the stable fixed point remains. For smaller values of g_{HTK} (middle and left panels), oscillations are present over an interval of g_{NL} values. This interval is a decreasing

function of g_{HTK} as summarized in Fig. 8D. There we show a two-parameter bifurcation diagram where the curve is the boundary between oscillatory and non-oscillatory behavior. For any choice of parameters that lies within the red shaded parabola-like region, oscillations are possible. For choices outside of this region, oscillations are not possible. The diagram clearly shows that the interval of g_{NL} values over which oscillations occurs shrinks as g_{HTK} is increased.

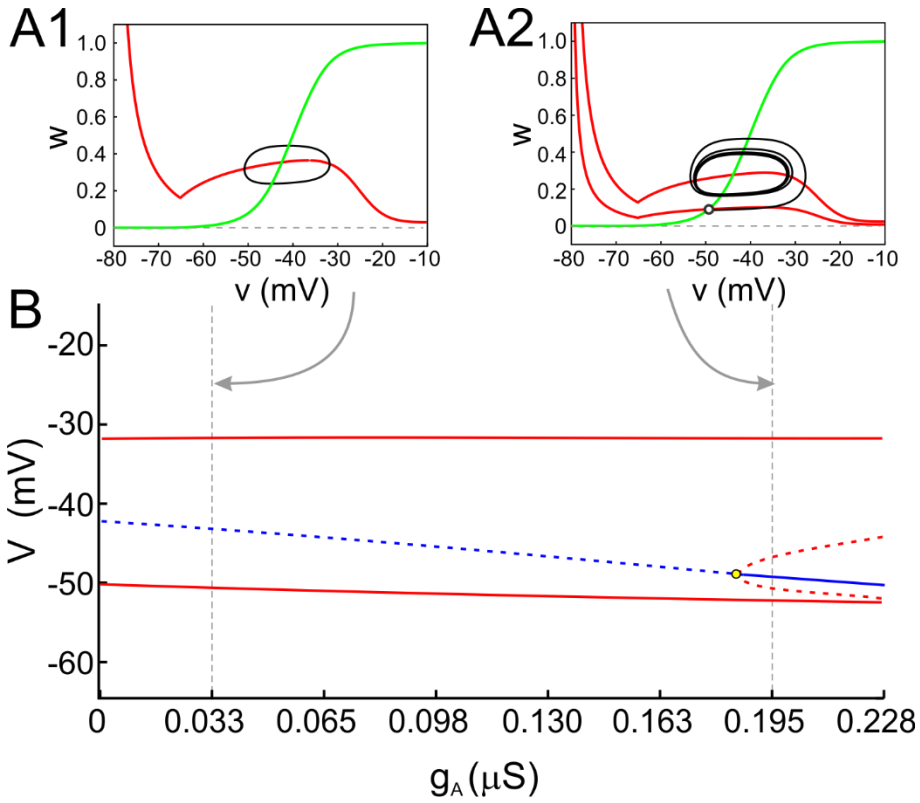

Figure 9 *The effect of I_A on the existence of oscillations*. **A1**.The projection onto the *v*-*w* phase plane for g_A=0.033 μS. No qualitative difference is found from the g_A = 0 μS case (shown in Fig. 8A1). The value of the third variable *h* (not shown) oscillates, but remains small. The *v*–nullcline shown is for the largest value of *h* along the periodic solution. The intersection of the projection of the *v* and *w*-nullclines is not a fixed point. **A2**. The projection onto the *v*-*w* phase plane at g_A=0.195 μS for which bistability exists between the periodic solution and a stable fixed point. The lower of the two *v*-nullclines occurs for *h* = 0.45 at the value corresponding to a stable fixed point (open circle). The upper of the two *v*-nullclines occurs at the largest *h* value along the periodic solution. **B**. Bifurcation diagram showing how the bistability of solutions depends on g_A. Arrows from panels A1 and A2 show the values of g_A used to produce those simulations. The unstable fixed point (dashed blue curve) undergoes a sub-critical Hopf bifurcation as g_A increases resulting in a stable fixed point and an unstable branch of periodic solutions.

Our experimental findings, as summarized in Fig. 7, suggest that I_A plays no role in generating oscillations, but may affect the properties of the oscillatory solution. Therefore, we investigated what role, if any, I_A may play in the generation of oscillations. With a non-zero value of I_A, equation (1) becomes three-dimensional and direct phase plane analysis is not possible. Thus, we now project the solution trajectory onto the *v*-*w* phase plane to study how the shape of the respective nullclines varies as a function of parameters associated with I_A. For example, Figure 9A1, shows the case where g_A= 0.0325 µS. Note that the projected nullclines look very much the same as those in Figure 8A1. As we varied the value of either g_A or the half-activation voltage of $h_\infty(v)$ we found little change in the shape of the projected nullclines. Thus, we concluded that the addition of I_A plays no role in whether a periodic solution exists, consistent with results of the prior sub-section. However, an interesting effect of a large I_A current was found to occur. A very strong *A*-current can induce bistability between a periodic solution and a stable fixed point. Figure 9A2 shows the case of g_A = 0.195 µS. For this parameter value, a stable periodic solution co-exists with a stable fixed point. The figure shows an example of a trajectory that starts at the stable fixed point where h = 0.45 (lower *v*-nullcline). Leaving the initial values of *v* and *w* unchanged, we switched to the initial condition h = 0. This has the effect of assigning a new initial condition in the full three-dimensional v-w-h phase space that is not a fixed point (though the location looks unchanged in the projection onto the v-w phase plane). The ensuing trajectory leaves that location and is seen to converge to the stable periodic orbit. The associated bifurcation diagram in Figure 9B shows that the stable fixed point loses stability through a subcritical Hopf bifurcation as g_A is decreased. The red, roughly horizontal curves depict the upper and lower limits of the periodic solution.

Note that the bifurcation diagram is also a projection onto the *v*-g_A space. In this projection, the value of h for the fixed point cannot be discerned. Indeed, the bifurcation diagram at g_A = 0.195 µS suggests that the stable periodic solution encloses the stable fixed point (Fig. 9B). But from the projected phase plane in Figure 9A2, it appears as if the stable periodic solution encloses an unstable fixed point. In reality, neither case is true. There is a stable fixed point whose projection in the *v*-*w* phase plane occurs at the intersection of the lower *v*-nullcline and the *w*-nullcline in Figure 9A2, and which occurs

for h = 0.45 (open circle). The intersection of the upper v-nullcline and the w-nullcline is not a fixed point, as the value of h is not constant along the periodic solution. Instead, it is oscillating near h = 0. In addition, the periodic solution has lower and upper v limits that are smaller and larger than the v value at the stable fixed point. This is why the bifurcation diagram misleadingly suggests that the stable periodic solution encloses the stable fixed point.

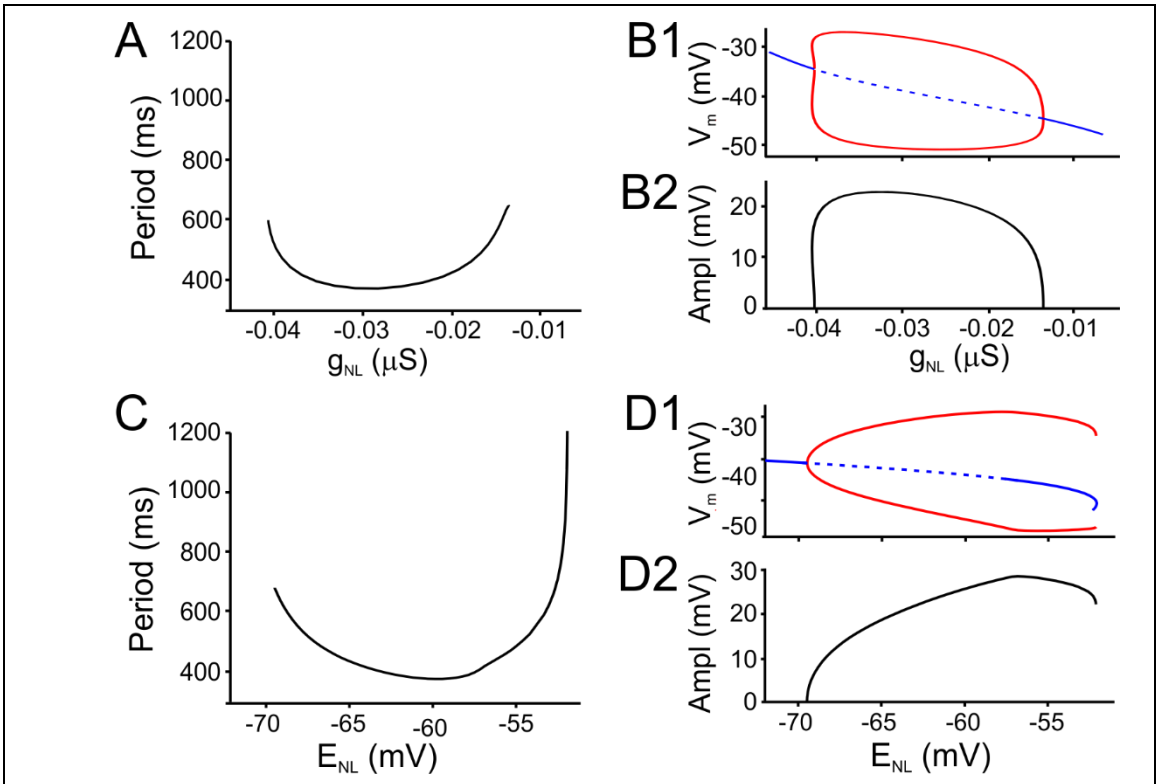

Figure 10 *Effect of I_{NL} parameters on oscillation period and amplitude.* **A, C**. Panels A and C are model analogs of Figs. 2B and 2D, showing how period depends on g_{NL} and E_{NL}, respectively. The simulations qualitatively match the behavior of the experimental system. **B1, D1**. Panels B1 and D1 plot the bifurcation diagrams obtained by respectively varying g_{NL} and E_{NL}. **B2, D2**. Panels B2 and D2 are model analogs of Figs. 2C and 2E, showing how oscillation amplitude depends on g_{NL} and E_{NL}, respectively. Amplitude is calculated as a difference between the minimum (bottom red) and maximum (top red) voltage for each parameter value in panels B1 and D1. The value E_{NL} =-65 mV in Panels A and B, g_{NL}=-0.0195 μS in Panel C and C, and g_A = 0 μS in all Panels.

Figure 10 shows model predictions for how the amplitude and period of oscillations depend on either g_{NL} (Figs. A1 and B1) or E_{NL} (Figs. A2 and B2). The model does a reasonable job in reproducing the dependence of period on both g_{NL} and E_{NL} (Figs.

10A1, 10A2), at least over a range of parameters (compare to Figs. 2B and 2D, respectively).

The dependence of the amplitude of oscillations on g_{NL} and E_{NL} (Figs. 10B2 and 10D2, respectively) is obtained by subtracting the upper value of voltage from the lower value (upper branch of red curve minus lower branch of red curve) in Figs. 10B1 and 10D1. The model does a poor job of describing the larger amplitude oscillations that arise in experiments for small absolute values of g_{NL} (compare Fig. 10B2 with Fig. 2C). Mathematically this is because oscillations in the model arise due a supercritical Hopf bifurcation, whereas those that arise in the experiments may correspond to a subcritical Hopf bifurcation. The dependence of amplitude on E_{NL} (compare Fig. 10D2 with Fig. 2E) is reasonably well described qualitatively by the model. Oscillations begin at small amplitude at low values of E_{NL} due to a super-critical Hopf bifurcation. There is a local maximum in the amplitude at higher values of E_{NL}, followed by a decrease in the amplitude just before oscillations cease to exist.

In sum, the simulations provide a theoretical framework to support the notion that the balance between high threshold outward currents and I_{NL} is critical to create pre-conditions for the existence of oscillations. Once this is in place, the simulations confirm that too much I_{HTK} (or too little total outward current) destroys this balance and thus can be used to determine which pyloric neurons can actually produce oscillations based on the I_{NL} protocol. The model also confirms that I_A does not appear to play a significant role in the generation or even modulation of oscillatory activity at least at relatively low amplitudes of the current.

Discussion

We have shown previously (Zhao et al. 2010) that the nearly linear and negatively-sloped portion of the inward modulator-activated current (I_{MI}) is the key element to produce oscillations in pacemaker cells of the pyloric central pattern generator. In (Bose et al. 2014), we addressed the question of what currents are minimally necessary to produce oscillatory activity in a single-cell model of a neural pattern generator. We did

so by examining a simplified model of an oscillator consisting of a high threshold K^+ current and a linear inward current that describes the behavior of this negative conductance component of I_{MI}, and which we call the negative-conductance leak current (I_{NL}). That work suggested, but left open, the question of how a balance between inward and distinct outward currents arises in pyloric neurons, and whether there are systematic differences in this balance between pacemaker and follower cells. Here, using both experiments and simulations, we provide evidence that pyloric neurons contain different levels of specific outward currents and that this may be the key distinction between what makes a neuron a pacemaker or a follower.

Experimentally, we find that one cell type, the PD neurons, which are considered part of the pacemaker groups of neurons in the network (Marder and Eisen 1984), are the only ones that can generate oscillations when driven by I_{NL}: PD neurons can sustain oscillations over a large but finite range of conductances and equilibrium potentials of I_{NL}. In contrast to the PD neurons, we find that no value of I_{NL} conductance (or combination of g_{NL} and E_{NL}) can induce oscillations in any of the follower neurons. These findings are consistent with the effect the endogenous neuromodulatory peptide proctolin on the pyloric network neurons (Hooper and Marder 1987; Zhao et al. 2010). Proctolin is one of the neuromodulators that activates I_{MI}, the current for which I_{NL} is a simplified (linear) version. Although proctolin produces oscillations in the pyloric pacemaker neurons, it does not produce oscillations in any of the synaptically isolated pyloric follower neurons (Hooper and Marder 1987; Zhao et al. 2010).

Because pyloric neurons have the same set of ionic currents (Schulz et al. 2006; Schulz et al. 2007; Temporal et al. 2012; Temporal et al. 2014), we explored the mechanisms that preclude endogenous oscillations in the follower neurons. We found that, in follower LP and VD neurons, high-threshold outward currents (I_{HTK}) are much too large, compared to the same currents in the PD neuron, to permit I_{NL}-induced oscillations. However, oscillations in both of these follower neuron types could be produced if I_{HTK} are reduced pharmacologically. These results suggests that, in order to be able to produce endogenous oscillations, a relative balance between the pacemaker current (for which I_{NL} is a surrogate) and the counteracting outward currents needs to be

maintained. Interestingly, we also observe that increasing the I_{NL} conductance alone cannot, at least in these cells, balance the high levels of outward currents. To address why the large outward currents cannot simply be balanced by increasing the inward currents, we used a simplified mathematical model. This model confirmed that there is a finite region in the g_{NL}-g_{HTK} space within which oscillations are possible (Fig. 8D). The bounds on this region result from either insufficient inward current when g_{HTK} is low (lower edge of oscillation region in Fig. 8D), or excessive leakiness of the cell when g_{HTK} is too high, which no level of g_{NL} can overcome to produce oscillations.

Several theoretical studies have suggested that a balance between inward and outward current is required for oscillatory activity to be generated (Doloc-Mihu and Calabrese 2014; Goldman et al. 2001; Hudson and Prinz 2010; Lamb and Calabrese 2013; Zhao and Golowasch 2012). In leech, it was shown that a close linear correlation between three currents, a leak current, a persistent K^+ current, and a persistent Na^+ current was required to ensure bursting oscillatory activity (Doloc-Mihu and Calabrese 2014; Lamb and Calabrese 2013). Although, in our case, the relationship between g_K and g_{NL} is not linear as in the leech studies, but rather bell-shaped and broad (Fig. 8D), those studies are consistent with ours in that relatively strict relationships must be maintained to ensure the generation of a number of features of activity, including oscillatory and bursting activity. Another example that supports the relationship between oscillatory activity and an inward/outward current balance is that of bursting pacemaker neurons in the rodent pre-Bötzinger respiratory center, in which a higher ratio of persistent Na^+ current to leak current (I_{NaP}/I_{leak}) is characteristic of pacemaker neurons, while a lower ratio is typical of follower neurons (Del Negro et al. 2002).

Studies with cultured STG neurons (Haedo and Golowasch 2006; Turrigiano et al. 1995) have shown that neurons may be programmed to maintain and even restore such relationships after the loss of oscillatory activity. In these studies, recovery of rhythmic activity in cultured crab STG neurons after dissociation required the reduction of I_{HTK}, and the increase in inward currents whose voltage dependence resembles that of I_{MI} and I_{NL}. These cells are capable of doing this over the course of hours to days in culture. Thus, we conclude that pacemaker activity in individual neurons involves a

careful balance, not simply a linear correlation, of an inward pacemaker current with some type of current, such as I_{HTK}, which promotes the recovery from depolarization.

In the STG, I_{HTK} is composed of two high-threshold currents, the delayed rectifier I_{Kdr} and the calcium-dependent I_{KCa}. The former is known to be involved in action potential generation, while I_{KCa} may more directly be involved in oscillatory activity (Haedo and Golowasch 2006; Soto-Trevino et al. 2005). Nevertheless, here (and earlier (Bose et al. 2014)) we showed that I_{Kdr} is also capable of generating oscillatory activity in conjunction with I_{MI} or I_{NL}. In other systems too, high-threshold K^+ currents have been shown to be essential elements of oscillatory mechanisms (e.g. Aplysia egg laying (Hermann and Erxleben 1987)) but the specific relationship with the inward currents engaged in oscillatory activity in that system have not been examined.

Interestingly, the transient *A*-current does not typically seem to be involved in pacemaker activity generation, as we confirmed in this study, even though its activation properties can be quite similar to those of high threshold K^+ currents. In our study, I_A has the same voltage-dependence of activation as I_{Kdr}, but only I_{Kdr} can participate in the generation of oscillatory activity (see also (Bose et al. 2014)). Thus, the differences in the kinetics and voltage dependencies of the inactivation variable are probably sufficient to determine or exclude its participation in pacemaker activity. Additionally, the transient I_A was not involved in the recovery of rhythmic activity in crab cultured cells (Haedo and Golowasch 2006), consistent with the result reported here.

Our modeling results also provide the basis to interpret and understand some of our experimental results regarding the dependence of period and amplitude on parameters associated with I_{NL}. They show that in most cases the results are qualitatively consistent over a subset of parameter values of the model. A comparison between Fig. 2B-E (experimental results) and Fig. 10 (model results) relative to how period and amplitude vary with g_{NL} and E_{NL}, for example, reveals a consistent relative independence of cycle period on g_{NL} (Fig. 2B). In the model, changes in g_{NL} simply shifted the *v*-nullcline up or down in the phase space, but left the overall balance of currents largely intact over a large range of values. As a result, neither period nor amplitude varies much (Figs. 10A and B). Variations due to changes in E_{NL} were also consistent across both experiment

and model. When E_{NL} becomes too small, the inward effect of I_{NL} is mitigated by the outward effect of I_{Kdr} (their reversal potentials are too close). Alternatively when E_{NL} is too large, the model cell is attracted to a higher level stable fixed point because the inward effect is too strong to be overcome (the driving force from I_{NL} is too large). The model also makes predictions about how oscillations are lost through specific kinds of bifurcations as g_{NL} or E_{NL} are varied. It would be of interest to test if these predictions are borne out experimentally, which would provide further insight into the mechanisms of rhythm generation in pacemaker neurons similar to pyloric pacemaker neurons.

In conclusion, we observe that a coordinated balance of high-threshold outward currents and inward pacemaker currents is required for the generation of oscillatory activity. This is consistent with previous experimental and theoretical observations, but here we show both approaches confirming this in the same biological system and using a minimal model that captures the essential features of these relationships.

References

Amarillo Y, Zagha E, Mato G, Rudy B, and Nadal MS. The interplay of seven subthreshold conductances controls the resting membrane potential and the oscillatory behavior of thalamocortical neurons. *Journal of Neurophysiology* 112: 393-410, 2014.
Amendola J, Woodhouse A, Martin-Eauclaire MF, and Goaillard JM. Ca(2)(+)/cAMP-sensitive covariation of I(A) and I(H) voltage dependences tunes rebound firing in dopaminergic neurons. *J Neurosci* 32: 2166-2181, 2012.
Anderson WD, Makadia HK, and Vadigepalli R. Molecular variability elicits a tunable switch with discrete neuromodulatory response phenotypes. *J Comput Neurosci* 40: 65-82, 2016.
Anirudhan A, and Narayanan R. Analogous synaptic plasticity profiles emerge from disparate channel combinations. *J Neurosci* 35: 4691-4705, 2015.
Bayliss DA, Viana F, and Berger AJ. Mechanisms underlying excitatory effects of thyrotropin-releasing hormone on rat hypoglossal motoneurons in vitro. *J Neurophysiol* 68: 1733-1745, 1992.
Bergquist S, Dickman DK, and Davis GW. A hierarchy of cell intrinsic and target-derived homeostatic signaling. *Neuron* 66: 220-234, 2010.
Blethyn KL, Hughes SW, Toth TI, Cope DW, and Crunelli V. Neuronal basis of the slow (<1 Hz) oscillation in neurons of the nucleus reticularis thalami in vitro. *J Neurosci* 26: 2474-2486, 2006.
Bose A, Golowasch J, Guan Y, and Nadim F. The role of linear and voltage-dependent ionic currents in the generation of slow wave oscillations. *J Comput Neurosci* 37: 229-242, 2014.
Brickley SG, Aller MI, Sandu C, Veale EL, Alder FG, Sambi H, Mathie A, and Wisden W. TASK-3 two-pore domain potassium channels enable sustained high-frequency firing in cerebellar granule neurons. *J Neurosci* 27: 9329-9340, 2007.
Cymbalyuk GS, Gaudry Q, Masino MA, and Calabrese RL. Bursting in leech heart interneurons: cell-autonomous and network-based mechanisms. *J Neurosci* 22: 10580-10592, 2002.
Del Negro CA, Koshiya N, Butera RJ, Jr., and Smith JC. Persistent sodium current, membrane properties and bursting behavior of pre-botzinger complex inspiratory neurons in vitro. *Journal of neurophysiology* 88: 2242-2250, 2002.
Doloc-Mihu A, and Calabrese RL. Identifying crucial parameter correlations maintaining bursting activity. *PLoS Comput Biol* 10: e1003678, 2014.
Dunmyre JR, Del Negro CA, and Rubin JE. Interactions of persistent sodium and calcium-activated nonspecific cationic currents yield dynamically distinct bursting regimes in a model of respiratory neurons. *Journal of computational neuroscience* 31: 305-328, 2011.
Egorov AV, Hamam BN, Fransen E, Hasselmo ME, and Alonso AA. Graded persistent activity in entorhinal cortex neurons. *Nature* 420: 173-178, 2002.
Ermentrout B. *Simulating, analyzing, and animating dynamical systems : a guide to XPPAUT for researchers and students*. Philadelphia: Society for Industrial and Applied Mathematics, 2002, p. xiv, 290 p.
Goaillard J-M, Taylor AL, Schulz DJ, and Marder E. Functional consequences of animal-to-animal variation in circuit parameters. *Nat Neurosci* 12: 1424-1430, 2009.

Goldman MS, Golowasch J, Marder E, and Abbott LF. Global structure, robustness, and modulation of neuronal models. *The Journal of neuroscience : the official journal of the Society for Neuroscience* 21: 5229-5238, 2001.
Golowasch J. Stability and Homeostasis in Small Network Central Pattern Generators. In: *Encyclopedia of Computational Neuroscience*, edited by Jaeger D, and Jung R. New York: Springer Verlag, 2015, p. 2858-2864.
Golowasch J, and Marder E. Ionic currents of the lateral pyloric neuron of the stomatogastric ganglion of the crab. *J Neurophysiol* 67: 318-331, 1992a.
Golowasch J, and Marder E. Proctolin activates an inward current whose voltage dependence is modified by extracellular Ca2+. *J Neurosci* 12: 810-817, 1992b.
Gray M, and Golowasch J. Voltage Dependence of a Neuromodulator-Activated Ionic Current. *eNeuro* 3: 2016.
Haedo RJ, and Golowasch J. Ionic mechanism underlying recovery of rhythmic activity in adult isolated neurons. *Journal of neurophysiology* 96: 1860-1876, 2006.
Hermann A, and Erxleben C. Charybdotoxin selectively blocks small Ca-activated K channels in Aplysia neurons. *J Gen Physiol* 90: 27-47, 1987.
Hooper SL, and Marder E. Modulation of the lobster pyloric rhythm by the peptide proctolin. *J Neurosci* 7: 2097-2112, 1987.
Hudson AE, and Prinz AA. Conductance ratios and cellular identity. *PLoS Comput Biol* 6: e1000838, 2010.
Jahnsen H, and Llinas R. Ionic basis for the electro-responsiveness and oscillatory properties of guinea-pig thalamic neurones in vitro. *The Journal of physiology* 349: 227-247, 1984.
Khorkova O, and Golowasch J. Neuromodulators, not activity, control coordinated expression of ionic currents. *J Neurosci* 27: 8709-8718, 2007.
Koizumi H, and Smith JC. Persistent Na+ and K+-dominated leak currents contribute to respiratory rhythm generation in the pre-Botzinger complex in vitro. *J Neurosci* 28: 1773-1785, 2008.
Lamb DG, and Calabrese RL. Correlated conductance parameters in leech heart motor neurons contribute to motor pattern formation. *PLoS One* 8: e79267, 2013.
Linsdell P, and Moody WJ. Na+ channel mis-expression accelerates K+ channel development in embryonic Xenopus laevis skeletal muscle. *J Physiol* 480 (Pt 3): 405-410, 1994.
Lu TZ, and Feng ZP. NALCN: a regulator of pacemaker activity. *Molecular neurobiology* 45: 415-423, 2012.
Lutas A, Lahmann C, Soumillon M, and Yellen G. The leak channel NALCN controls tonic firing and glycolytic sensitivity of substantia nigra pars reticulata neurons. *Elife* 5: 2016.
MacLean JN, Zhang Y, Johnson BR, and Harris-Warrick RM. Activity-independent homeostasis in rhythmically active neurons. *Neuron* 37: 109-120, 2003.
Marder E, and Eisen JS. Electrically coupled pacemaker neurons respond differently to same physiological inputs and neurotransmitters. *J Neurophysiol* 51: 1362-1374, 1984.
McCormick DA, and Huguenard JR. A model of the electrophysiological properties of thalamocortical relay neurons. *Journal of Neurophysiology* 68: 1384-1400, 1992.
Pang DS, Robledo CJ, Carr DR, Gent TC, Vyssotski AL, Caley A, Zecharia AY, Wisden W, Brickley SG, and Franks NP. An unexpected role for TASK-3 potassium

channels in network oscillations with implications for sleep mechanisms and anesthetic action. *Proc Natl Acad Sci U S A* 106: 17546-17551, 2009.
Rekling JC, Funk GD, Bayliss DA, Dong XW, and Feldman JL. Synaptic control of motoneuronal excitability. *Physiol Rev* 80: 767-852, 2000.
Roffman RC, Norris BJ, and Calabrese RL. Animal-to-animal variability of connection strength in the leech heartbeat central pattern generator. *J Neurophysiol* 107: 1681-1693, 2012.
Schulz DJ, Goaillard JM, and Marder E. Variable channel expression in identified single and electrically coupled neurons in different animals. *Nat Neurosci* 9: 356-362, 2006.
Schulz DJ, Goaillard JM, and Marder EE. Quantitative expression profiling of identified neurons reveals cell-specific constraints on highly variable levels of gene expression. *Proc Natl Acad Sci U S A* 104: 13187-13191, 2007.
Selverston AI, Russell DF, and Miller JP. The stomatogastric nervous system: structure and function of a small neural network. *Prog Neurobiol* 7: 215-290, 1976.
Soto-Trevino C, Rabbah P, Marder E, and Nadim F. Computational model of electrically coupled, intrinsically distinct pacemaker neurons. *J Neurophysiol* 94: 590-604, 2005.
Srikanth S, and Narayanan R. Variability in State-Dependent Plasticity of Intrinsic Properties during Cell-Autonomous Self-Regulation of Calcium Homeostasis in Hippocampal Model Neurons(1,2,3). *eNeuro* 2: 2015.
Swensen AM, and Marder E. Multiple peptides converge to activate the same voltage-dependent current in a central pattern-generating circuit. *J Neurosci* 20: 6752-6759, 2000.
Talley EM, Lei Q, Sirois JE, and Bayliss DA. TASK-1, a two-pore domain K+ channel, is modulated by multiple neurotransmitters in motoneurons. *Neuron* 25: 399-410, 2000.
Temporal S, Desai M, Khorkova O, Varghese G, Dai A, Schulz DJ, and Golowasch J. Neuromodulation independently determines correlated channel expression and conductance levels in motor neurons of the stomatogastric ganglion. *Journal of Neurophysiology* 107: 718-727, 2012.
Temporal S, Lett KM, and Schulz DJ. Activity-dependent feedback regulates correlated ion channel mRNA levels in single identified motor neurons. *Curr Biol* 24: 1899-1904, 2014.
Turrigiano G, LeMasson G, and Marder E. Selective regulation of current densities underlies spontaneous changes in the activity of cultured neurons. *J Neurosci* 15: 3640-3652, 1995.
van den Top M, Lee K, Whyment AD, Blanks AM, and Spanswick D. Orexigen-sensitive NPY/AgRP pacemaker neurons in the hypothalamic arcuate nucleus. *Nat Neurosci* 7: 493-494, 2004.
Vandermaelen CP, and Aghajanian GK. Electrophysiological and pharmacological characterization of serotonergic dorsal raphe neurons recorded extracellularly and intracellularly in rat brain slices. *Brain Res* 289: 109-119, 1983.
Xu XF, Tsai HJ, Li L, Chen YF, Zhang C, and Wang GF. Modulation of leak K(+) channel in hypoglossal motoneurons of rats by serotonin and/or variation of pH value. *Sheng Li Xue Bao* 61: 305-316, 2009.

Yamada-Hanff J, and Bean BP. Persistent sodium current drives conditional pacemaking in CA1 pyramidal neurons under muscarinic stimulation. *J Neurosci* 33: 15011-15021, 2013.
Zhao S, and Golowasch J. Ionic current correlations underlie the global tuning of large numbers of neuronal activity attributes. *J Neurosci* 32: 13380-13388, 2012.
Zhao S, Golowasch J, and Nadim F. Pacemaker neuron and network oscillations depend on a neuromodulator-regulated linear current. *Frontiers in behavioral neuroscience* 4: 21, 2010.